

Title: Tumor Absorbed Dose for non-Hodgkin's Lymphoma Patients treated with the novel anti-CD37 antibody radionuclide conjugate ^{177}Lu -lilotomab satetraxetan

Authors: Johan Blakkisrud¹, Ayca Løndalen², Anne C. T. Martinsen^{1,3}, Jostein Dahle⁴, Jon E. Høltedahl¹, Tore Bach-Gansmo², Harald Holte⁵, Arne Kolstad⁵ & Caroline Stokke^{1,6*}

¹The Intervention Centre, Oslo University Hospital, Oslo, NORWAY

²Department of Radiology and Nuclear Medicine, Oslo University Hospital, Oslo, NORWAY

³The Department of Physics, University of Oslo, Oslo, NORWAY

⁴Nordic Nanovector ASA, Oslo, NORWAY

⁵Department of Oncology, The Norwegian Radium Hospital, Oslo University Hospital, Oslo, NORWAY

⁶Department of Life Science and Health, Oslo and Akershus University College of Applied Sciences, Oslo, NORWAY

Disclaimer: The study was sponsored by Nordic Nanovector ASA. Johan Blakkisrud was in part supported by grants from Nordic Nanovector ASA. Harald Holte and Arne Kolstad were both in part supported by grants from the Norwegian Cancer society.

*Corresponding author: Caroline Stokke, The Intervention Centre, Oslo University Hospital,
P.box 4950 Nydalen,0424 Oslo, NORWAY, Telephone:(0047)23071737, Fax:(0047)23070110,
Email:carsto@ous-hf.no

First author: Johan Blakkisrud, The Intervention Centre, Oslo University Hospital,P.box 4950
Nydalen,0424 Oslo, NORWAY, Telephone:(0047)48146588, Fax:(0047)23070110,
Email:johbla@ous-hf.no

Word count: 4998

Running title: ¹⁷⁷Lu-lilotomab satetraxetan Tumor Doses

ABSTRACT

¹⁷⁷Lu-lilotomab satetraxetan is a novel antibody radionuclide conjugate (ARC) currently tested in a phase 1/2a first-in-human dosage escalation trial for patients with relapsed CD37+ indolent non-Hodgkin's lymphoma. The aim of this work was to develop dosimetric methods and calculate tumor absorbed radiation doses for patients treated with ¹⁷⁷Lu-lilotomab satetraxetan.

Methods: Patients were treated at escalating injected activities (10, 15 and 20 MBq/kg) of ¹⁷⁷Lu-lilotomab satetraxetan and with different pre-dosing; with or without 40 mg unlabeled lilotomab. Eight patients were included for the tumor dosimetry study. Tumor radioactivity concentrations were calculated from Single Photon Emission Computer Tomography (SPECT) acquisitions at multiple time points, and tumor masses were delineated from corresponding Computer Tomography (CT) scans. Tumor absorbed doses were then calculated using the OLINDA sphere model. To perform voxel dosimetry, the SPECT/CT data and an in-house developed MATLAB program were combined to investigate the dose rate homogeneity. **Results:** Twenty-six tumors in 8 patients were ascribed a mean tumor absorbed dose. Absorbed doses ranged from 75 cGy to 794 cGy with a median of 268 cGy across different dosage levels and different pre-dosing. A significant correlation between the dosage level and tumor absorbed dose was found. Twenty-one tumors were included for voxel dosimetry, and parameters describing dose-volume coverage calculated. The investigation of intra-tumor voxel doses indicates that mean tumor dose is correlated to these parameters. **Conclusion:** Tumor absorbed doses for patients treated with ¹⁷⁷Lu-lilotomab satetraxetan are comparable to doses reported for other radioimmunotherapy compounds. Although the inter-tumor variability was considerable, a correlation between tumor

dose and patient dosage level was found. Our results indicate that mean dose may be used as the sole dosimetric parameter on the lesion level.

Key words: Tumor absorbed dose, antibody radionuclide conjugate, non-Hodgkin's lymphoma, dose-volume-histogram

INTRODUCTION

Non-Hodgkin's lymphoma (NHL) represents a diverse group of malignant hematological disorders. In the United States NHL is the fifth most common cancer with 71 850 estimated new cases in 2015 (1). Most NHLs derive from B-lymphocytes and express B-cell antigens like CD19, CD20 and CD37. Relapses are common after conventional treatments for NHL, such as external beam radiation therapy (EBRT) or immunochemotherapy (2). Radioimmunotherapy, or ARC-therapy, is a treatment that utilizes targeting antibodies linked to a radionuclide. Two ARCs are currently approved by the US Food and Drug administration; ¹³¹Iodine-tositumomab (Bexxar) and ⁹⁰Yttrium-ibritumomab-tiuxetan (Zevalin) (3). Both agents consist of a monoclonal antibody specific for the CD20 antigen, with a beta-emitting radionuclide attached. Considering that these two ARCs are used after patients have been treated with several rounds of rituximab, which also targets CD20, a conjugate that targets a different antigen would be desirable. ¹⁷⁷Lu-lilotomab satetraxetan (Betalutin®, previously ¹⁷⁷Lu-DOTA-HH1) is a novel ARC, where the lilotomab antibody binds to CD37 antigens expressed on malignant B-cells (4,5). Lutetium-177 is a beta-emitter with mean beta energy of 0.133 MeV (mean and max beta-range in water: 0.25 and 1.9 mm) that also emits photons with gamma-energies of 113 keV (6 %) and 208 keV (11 %), which permits gamma camera and SPECT/CT imaging as a means of dosimetry (6).

Insight in absorbed dose to tumors is of high importance to assess treatment efficiency. In EBRT, dose planning to optimize tumor dose and dose to organs at risk is considered essential. Over the last years, there has been increased focus on dosimetry also for internal emitters. While the Committee on Medical Internal Radiation Dose (MIRD) pamphlets suggest guidelines for normal tissue and tumor dosimetry, there is still a lack of consensus on how and when to perform

dose calculations and how to evaluate doses for most radionuclide therapies. ^{131}I -tositumomab SPECT-based tumor dosimetry was initially done by daily planar imaging supported by a single SPECT-acquisition (7,8). Later, more comprehensive dosimetric models were developed (9), including methods to analyze intra-tumor dose inhomogeneity. SPECT/CT images from multiple time points were used to obtain a predictive relationship between progression-free survival and mean tumor dose (10,11).

In order to evaluate not solely the mean dose for a tumor, but also identify parts of the tumor receiving too low doses, dose-volume-histograms (DVHs) are routinely used in EBRT. Voxel-based dosimetry assigning each voxel an absorbed dose is the foundation for creating DVHs. To do this accurately requires tracking of the radioactivity in each voxel over time, which for tumors subjected to deformation can be a challenging task. A dose-rate-volume-histogram (DRVH) will instead depict the dose rates in a tumor at an instant moment.

The aim of the current work was to develop dosimetric procedures and establish tumor absorbed doses for patients in the phase 1 study of ^{177}Lu -lilotomab satetraxetan; both on a mean tumor and on a tumor voxel level.

MATERIALS AND METHODS

Patient Population and Treatment

A total of 8 patients with relapsed indolent NHL treated in the phase 1 LYMRIT-37-01 trial were included for tumor dosimetry. This study was approved by the regional ethical committee and all patients had signed informed consent. The participants received a single injection of ^{177}Lu -lilotomab satetraxetan. In order to deplete normal B-cells, two infusions of rituximab (375 mg/m^2) were given at 4 and 3 weeks before administration of ^{177}Lu -lilotomab satetraxetan. In addition, two different pre-dosing regimes were tested; patients in arm 1 were pre-dosed with 40 mg unlabeled antibody (lilotomab) 4 hours prior to injection while patients in arm 2 were not. ^{177}Lu -lilotomab satetraxetan was administered at a fixed amount of activity per body weight (dosage level), ranging from 10 to 20 MBq/kg (Table 1). Body Surface Area (BSA) was calculated using the Dubois and Dubois method (12).

Image Acquisition and Reconstruction

All patients were imaged using a dual headed Symbia T16 SPECT/CT scanner (Siemens, Erlangen, Germany), equipped with a 3/8-inch-thick NaI crystal and a medium energy collimator. Patients in arm 1 underwent 2 SPECT/CT-scans; 96 and 168 hours after ^{177}Lu -lilotomab satetraxetan. Patients in arm 2 had 3 SPECT/CT scans; after 24, 96 and 168 hours. Figure 1 shows SPECT/CT images for one of the patients. Energy windows were centered at the 113 and 208 keV photon peaks with 20 % window width. Two lower scatter windows with a 20 % width were used. Scans were performed with 2 x 32 projections, each of 45 seconds frame length in a non-circular orbit in step and shoot mode. Attenuation and scatter corrections were performed

using the vendor's software (Siemens Medical Esoft, Erlangen, Germany). An ordered subset expectation maximization reconstruction was used, having 4 iterations and 16 subsets and a Gaussian filtration of 4 mm. Matrix size was 128 by 128 with a pixel size of 4.8 mm. Collimator compensation was not utilized. CT scans were performed with 30 mAs and 130 keV tube voltage. Matrix size was 512 by 512 with 3 mm slice thickness.

Scanner Calibration and Phantom Measurements

SPECT/CT data were analyzed using the software program PMOD version 3.6 (PMOD Industries, Zurich, Switzerland). A calibration factor was found using an anthropomorphic Torso Model ECT/TOR/P water-filled phantom (Data Spectrum Corporation, USA) containing an insertion with 106.3 MBq of ^{177}Lu -lilotomab satetraxetan in 1.2 l water. Resolution was measured by a capillary tube. A series of phantom measurements with spherical insertions (2, 4, 8, 16 and 113 ml) was also performed. Initial activity concentration in the spheres was 0.69 MBq/ml, with subsequent activity concentrations being 0.37, 0.13 and 0.03 MBq/ml. Volumes of Interest (VOIs) were drawn with 10 and 20 mm margins around the sphere walls. In addition, "manually" defined VOIs of 10-20 mm margins were drawn to include all counts seemingly originating from the spheres.

Lesion Delineation

A total of 26 tumors were included. Lesions were included based on the following criteria; visual identification of lesion on CT and activity on SPECT as well as a volume of minimum 1.5 ml. Delineation was primarily carried out on the scan performed at 96 hours. Two individual VOIs were defined for each tumor, both drawn manually in a slice by slice manner by an experienced nuclear medicine specialist. An anatomical VOI, VOI_{CT} , was drawn tangent to the

tumor edge. A functional VOI, VOI_{SPECT}, was drawn on the SPECT-image with a manually defined margin. These two VOIs were then transferred to the 168 hour and the 24 hour data sets.

Dose Calculation

The counts in VOI_{SPECT} were converted to activity. A time-activity curve was calculated from two time points (3 in arm 2 for comparison) by assuming a mono-exponential clearance with an effective half-life t_{eff} . Following the MIRD-formalism, the total number of disintegrations is:

$$\tilde{A} = \int_0^{\infty} A_0 e^{-\frac{\ln(2)}{t_{\text{eff}}}t} dt.$$

Absorbed dose is then calculated by

$$\bar{D} = \frac{\tilde{A}}{m_{CT}} \bar{S}$$

where m_{CT} is the tumor mass, found by the volume of VOI_{CT} and assuming uniform mass density equal to water. \bar{S} is a dose factor of $8.56 \cdot 10^{-5}$ GyKg/MBqh calculated from the OLINDA/EXM uniform density sphere model for a sphere of 10 g (13). The error of \bar{S} for the tumor volumes in this work is about 1 %. To compare doses across dosage levels, \bar{D} was normalized by administered activity.

Voxel Dosimetry

The voxel dosimetry was carried out by the local deposition method (14). Tumors larger than 4 ml were included for voxel dosimetry; 21 tumors in total. SPECT data and the anatomical

VOI were exported from PMOD and analyzed using in-house developed software written in MATLAB version 2015a (Mathworks Inc, Natick, USA). The SPECT activity data were multiplied with a dose conversion constant, based on the assumption of 0.133 MeV energy absorbed per disintegration. The dose rate maps were further analyzed by constructing cumulative dose-rate-volume-histograms (cDRVHs).

Statistics

A Mann-Whitney U-test was performed to investigate if tumor doses for arm 1 and arm 2 differed. A null-hypothesis of equal populations with a rejection level of 0.05 was set. The relationship between mean absorbed dose and the following parameters was investigated for tumors belonging to patients in arm 1: activity per body weight (dosage level), total administered activity, activity per BSA and tumor mass. The Spearman rank correlation coefficient with a significance level of $p < 0.05$ was used. Relationship between mean dose and dose rate covering the 10, 50 and 90 % of the tumor volume ($D_{10\%}$, $D_{50\%}$ and $D_{90\%}$, respectively) for both arm 1 and 2 was investigated using the Spearman rank test. All statistical calculations were conducted using MATLAB version 2015a (Mathworks Inc, Natick, USA).

RESULTS

Phantom Studies and a Margin-Based Quantification Method

The calibration factor was determined to be 15.9 Bq/counts, the full width at half maximum was measured to 19.2 mm. The results of the phantom acquisitions are found in Supplementary Table 1. A 10 mm margin generally led to an underestimation of activity and 20 mm to an overestimation. The latter was due to contribution from the surrounding spheres. Mean errors for manually defined margins, the quantification method used for the patient tumors, range from -3.5 to -1.3 %.

Mean Tumor Absorbed Doses

A total of 26 tumors from 8 patients were included for dosimetry (Table 2). Inter-patient variations were observed with tumor absorbed dose ranging from 75 cGy to 794 cGy across different dosage levels. For patients included in arm 1 the mean overall tumor absorbed dose was 2.2 mGy/MBq (range 0.5 – 5.3 mGy/MBq). The patients in arm 2 received a mean overall tumor absorbed dose of 2.5 mGy/MBq (range 0.9 – 5.1 mGy/MBq). There was no statistical significant difference between doses in arm 1 and 2 ($p = 0.60$), indicating that the 40 mg pre-dosing did not change the tumor uptake of ^{177}Lu -lilotomab satetraxetan. For patients in the 10 MBq/kg group, the 15 MBq/kg group and the 20 MBq/kg group in arm 1, the median dose was 120 cGy, 302 cGy, and 323 cGy, respectively. For patients in the 15 MBq/kg group in arm 2 the median dose was 263 cGy.

The tumor absorbed dose increased significantly with the administered activity divided by body weight (dosage level) in arm 1 (Fig. 2A). In contrast, the tumor absorbed dose did not

increase with total injected activity (Fig. 2B). Figure 2C shows tumor absorbed dose plotted against administered activity divided by BSA. The tumor mass varied, with an average of 10.0 g (Table 2). There was no statistical significant relationship between tumor absorbed dose and tumor mass (Fig. 3).

The largest intra-patient variation in arm 1 in absolute dose values was found in patient 7, displaying tumor absorbed doses ranging from 319 to 794 cGy. Patient 13 displayed the largest variation in arm 2. For all patients in arm 1 the intra-patient dose ratio (the ratio between the highest and lowest tumor dose in the patient) were larger than 2:1. For 3 of 6 patients the same ratio was larger than 2.5:1.

Dose-Rate-Volume-Histograms

Figure 4 illustrates a dose rate map and the accompanying cDRVH for tumor 5b. The cDRVHs for all tumors included are shown in Figure 5. The cDRVHs differ somewhat in shape. For example, tumor 5c shows a long plateau and a very steep fall down to zero, indicating a fairly homogenous dose. In contrast, tumor 5a has a more gradual decrease, indicating a larger spread in dose rates in different parts of the tumor.

Table 3 quantifies the shape of cDRVH. The minimum dose rates covering 10, 50 and 90 % of the tumor volumes are shown. A strong correlation was found between mean absorbed dose and the dose rate thresholds $D_{10\%}$ ($r = 0.77$ $p < 0.0001$) $D_{50\%}$ ($r = 0.82$ $p < 0.0001$) and $D_{90\%}$ ($r = 0.58$ $p = 0.006$).

DISCUSSION

Knowledge about tumor absorbed dose is fundamental for the evaluation of new ARC treatments. Here we have calculated both mean tumor dose and dose rate on the voxel-level for a first-in-human study of ^{177}Lu -lilotomab satetraxetan.

The median dose across the patient population was 268 cGy. Even though lymphomas are radiation sensitive, this can be considered a relatively low radiation dose compared to doses in EBRT (15). However, for other ARCs absorbed dose in the same order of magnitude as the doses found here have been reported. For ^{131}I -tositumomab the tumor doses have ranged from 102-711 cGy (16). In a study which correlated tumor absorbed dose and progression-free survival for ^{131}I -tositumomab treatment a significant difference in progression-free survival was observed when using a dose threshold of 200 cGy (11). This 200 cGy threshold is slightly below the estimated median dose delivered to patients in our study. Tumor dose estimates for ^{90}Y -ibritumomab-tiuxetan were found in the range of 580 to 6700 cGy in one study (17). There is more uncertainty around these data, since the dosimetry was based on planar imaging of a substitute ligand with the radionuclide indium-111. However, the concept of absorbed dose by itself is not suitable for comparing external and internal radiation therapy or even internal emitters loaded with different radionuclides. The differences in both physical and biological parameters make direct evaluation of both tumor and normal tissue absorbed doses for ^{177}Lu -lilotomab satetraxetan somewhat challenging. Still, our results indicate that red marrow absorbed doses can be kept below 200 cGy with the above-mentioned tumor absorbed doses (Blakkisrud et. al, submitted corresponding manuscript).

Correlation of tumor absorbed dose and patient dosage level demonstrated a significant increase in tumor dose for increasing dosage level (Fig. 2A). This increase indicates that the chosen dosage regime ensures higher tumor dose for increasing levels of activity per body weight, regardless of patient shape. We also investigated whether other dosage regimes could demonstrate better prediction of tumor dose. Dosage with a fixed activity is known from treatment of for example thyroid cancer (18) and dosage determined by BSA adjusted activity from a study of ^{177}Lu -DOTA-rituximab (19). However, our results indicate that these two other theoretical regimes would not deliver higher tumor absorbed doses if the patient dosage was increased. While the current dosage method (activity/body weight) seems the best suited, a rather low r-value of 0.56 for the tumor dose and patient dosage level correlation may suggest that there are more optimal means for delivering this treatment.

Intra-patient variability in absorbed tumor dose was observed; most striking in patient 13. This patient has both the minimum and maximum tumor absorbed dose in the 15 MBq/kg groups considering both arm 1 and 2. Interestingly, these two tumors had almost identical size and were both located in the axillary area contralaterally (Fig. 1). A possible explanation for the intra-patient variability could be differences in expression of the target antigen CD37. Another explanation may be different vascularization, but the lack of correlation between tumor dose and mass in our study contradicts this hypothesis (Fig. 3).

In this study, quantification of radioactivity uptake has been investigated using spheres imitating lesions and larger margin-based VOIs to allow for spill-out effects of the imaging system and patient motion during the long acquisitions. The results indicate a well-functioning quantification routine and are similar to previous results for lutetium-177 (20). Quantification can alternatively be performed by the use of recovery coefficients. This scheme is often chosen for quantification of iodine-131 as the energy of this nuclide is higher (21), but has also been found

suited for lutetium-177 peptide-receptor-radionuclide therapy (22). As we have much lower activity concentration and virtually no background activity, the large VOI method was here preferred to allow some blurring due to patient motion. Mono-exponential activity clearance is an approximation that has been used under similar conditions (23-25). The limited number of data points for the tumors belonging to patients in arm 1 can introduce uncertainty for the time-activity curves. Patients in arm 2 were scanned 3 times, potentially improving this factor. While the calculated dose using 2 or 3 time points for these patients were found having a mean error of 5.5 % ($n = 7$, maximum error 16 %, data not shown), fit-related parameters probably introduce the larger uncertainty of this study. The mean tumor dose calculation takes into account the contribution from radiation inside the tumor, neglecting cross fire from surrounding tissue. Use of the OLINDA-unit-sphere model for tumors has been compared to a full Monte Carlo simulation for iodine-131 (16). Excellent agreement for self-dose, and good agreement when cross fire was included, was then found. As lutetium-177 has both shorter path lengths of the electrons and considerably less cross fire, an even better agreement is assumed.

To accurately determine DVHs, activity of the individual voxels must be tracked between multiple time points, in analog to the time activity curve used in the mean tumor absorbed dose model. Temporal tracking has been investigated by radial deformations of tumors (10). Our dose rate maps only depict the doses at day 4, and while not providing the complete dosimetric picture, they are neither prone to mismatched registration of maps from different time points. Another method for voxel dosimetry has been based on calculation of the voxel dose rates at a single time point and assumption of the same activity wash-out for each voxel as for the whole tumor (26). Combining the cDRVHs (Fig. 5) and the effective half-lives (Table 2) here provides analog information. The shape of the cDVHs would remain exactly the same as the cDRVHs, and all statistical correlations between mean dose and $D_{xx\%}$ identical.

Our analysis of the dose rate maps suggests that inter- and intra-tumor variability exist on the voxel level. While mean absorbed dose values can be useful, knowledge of how this dose is distributed must be considered before meaningful interpretations can be made. This is especially important for response evaluation; a high mean dose can be found while parts of the tumor still receive zero absorbed dose. Here, a strong monotonic relationship has been found between the dose rates covering 50 and 10 % of the volume and the mean absorbed doses (Table 3). If the mean dose value is predictive of the other dose-volume parameters, these comprehensive voxel analyses are perhaps redundant.

CONCLUSION

Dosimetric methods following the MIRD-formalism for internal emitters have been developed on two levels; for whole tumors considering the mean absorbed dose, and on a voxel-level using cumulative dose rate volume histograms. The methods correlate with each other, indicating that one of them could be rendered redundant. Tumor absorbed doses increase with dosage level for patients treated with ^{177}Lu -lilotomab satetraxetan, and are comparable to other ARCs.

DISCLOSURE

This study was sponsored by Nordic Nanovector ASA. Johan Blakkisrud was in part supported by grants from Nordic Nanovector ASA. Harald Holte and Arne Kolstad were both in part supported by grants from the Norwegian Cancer Society.

ACKNOWLEDGMENTS

We thank the personnel at the Nuclear Medicine section at Oslo University Hospital for technical assistance with the acquisitions. Stine Nygaard, study nurse at the Department of Oncology, is also greatly acknowledged. The authors wish to thank the anonymous reviewers for their suggestions.

REFERENCES

1. Siegel RL, Miller KD, Jemal A. Cancer statistics, 2015. *CA Cancer J Clin.* 2015;65:5-29.
2. Chao MP. Treatment challenges in the management of relapsed or refractory non-Hodgkin's lymphoma – novel and emerging therapies. *Cancer Manag Res.* 2013;5:251-269.
3. Jacene HA, Filice R, Kasecamp W, Wahl RL. Comparison of ⁹⁰Y-ibritumomab tiuxetan and ¹³¹I-tositumomab in clinical practice. *J Nucl Med.* 2007;48:1767-1776.
4. Repetto-Llamazares AHV, Larsen RH, Patzke S, et al. Targeted cancer therapy with a novel anti-CD37 beta-particle emitting radioimmunoconjugate for treatment of non-Hodgkin lymphoma. *PLoS ONE.* 2015;10:1-19.
5. Smeland E, Funderud S, Ruud E, Kiil Blomhoff H, Godal T. Characterization of two murine monoclonal antibodies reactive with human B cells: their use in a high-yield, high-purity method for isolation of B cells and utilization of such cells in an assay for B-cell stimulating factor. *Scand J Immunol.* 1985;21:205-214.

6. Jødal L. Beta emitters and radiation protection. *Acta Oncol.* 2009;48:308-313.

7. Koral KF, Dewaraja Y, Li J, et al. Initial results for hybrid SPECT-conjugate-view tumor dosimetry in ¹³¹I-anti-B1 antibody therapy of previously untreated patients with lymphoma. *J Nucl Med.* 2000;41:1579-1586.

8. Koral KF, Dewaraja Y, Li J, et al. Update on hybrid conjugate-view SPECT tumor dosimetry and response in ¹³¹I-tositumomab therapy of previously untreated lymphoma patients. *J Nucl Med.* 2003;44:457-464.

9. Sgouros G, Frey E, Wahl R, He B, Prideaux A, Hobbs R. 3-D imaging based, radiobiological dosimetry. *Semin Nucl Med.* 2008;38:321-334.

10. Dewaraja YK, Schipper MJ, Roberson PL, et al. ¹³¹I-tositumomab radioimmunotherapy: initial tumor dose–response results using 3-dimensional dosimetry including radiobiologic modeling. *J Nucl Med.* 2010;51:1155-1162.

11. Dewaraja YK, Schipper MJ, Shen J, et al. Tumor-absorbed dose predicts progression-free survival following ¹³¹I-tositumomab radioimmunotherapy. *J Nucl Med.* 2014;55:1047-1053.

12. Bois D, Bois E. Clinical calorimetry: tenth paper: a formula to estimate the approximate surface area if height and weight be known. *Arch Intern Med.* 1916;17:863-871.

13. Stabin MG, Konijnenberg MW. Re-evaluation of absorbed fractions for photons and electrons in spheres of various sizes. *J Nucl Med.* 2000;41:149-160.

14. Pasciak AS, Bourgeois AC, Bradley YC. A comparison of techniques for (90)Y PET/CT image-based dosimetry following radioembolization with resin microspheres. *Front Oncol.* 2014;4:121.

15. Lowry L, Smith P, Qian W, et al. Reduced dose radiotherapy for local control in non-Hodgkin lymphoma: a randomised phase III trial. *Radiother Oncol.* 2011;100:86-92.

16. Howard DM, Kearfott KJ, Wilderman SJ, Dewaraja YK. Comparison of I-131 radioimmunotherapy tumor dosimetry: unit density sphere model versus patient-specific Monte Carlo calculations. *Cancer Biother Radiopharm.* 2011;26:615-621.

17. Wiseman GA, White CA, Stabin M, et al. Phase I/II 90Y-Zevalin (yttrium-90 ibritumomab tiuxetan, IDEC-Y2B8) radioimmunotherapy dosimetry results in relapsed or refractory non-Hodgkin's lymphoma. *Eur J Nucl Med.* 2000;27:766-777.

18. Freitas JE, Gross MD, Ripley S, Shapiro B. Radionuclide diagnosis and therapy of thyroid cancer: current status report. *Semin Nucl Med.* 1985;15:106-131.

19. Forrer F, Oechsli-Oberholzer C, Campana B, et al. Radioimmunotherapy with ¹⁷⁷Lu-DOTA-Rituximab: final results of a phase I/II study in 31 patients with relapsing follicular, mantle cell, and other indolent B-cell lymphomas. *J Nucl Med.* 2013;54:1045-1052.

20. Beauregard J-M, Hofman MS, Pereira JM, Eu P, Hicks RJ. Quantitative (¹⁷⁷)Lu SPECT (QSPECT) imaging using a commercially available SPECT/CT system. *Cancer Imaging.* 2011;11:56-66.

21. Dewaraja YK, Frey EC, Sgouros G, et al. MIRD pamphlet no. 23: quantitative SPECT for patient-specific 3-dimensional dosimetry in internal radionuclide therapy. *J Nucl Med.* 2012;53:1310-1325.

22. Ilan E, Sandström M, Wassberg C, et al. Dose response of pancreatic neuroendocrine tumors treated with peptide receptor radionuclide therapy using ¹⁷⁷Lu-DOTATATE. *J Nucl Med.* 2015;56:177-182.

23. DeNardo DA, DeNardo GL, Yuan A, et al. Prediction of radiation doses from therapy using tracer studies with iodine-131-labeled antibodies. *J Nucl Med.* 1996;37:1970-1975.
24. Buckley SE, Saran FH, Gaze MN, et al. Dosimetry for fractionated 131I-mIBG therapies in patients with primary resistant high-risk neuroblastoma: preliminary results. *Cancer Biother Radiopharm.* 2007;22:105-112.
25. Sandström M, Garske U, Granberg D, Sundin A, Lundqvist H. Individualized dosimetry in patients undergoing therapy with 177Lu-DOTA-D-Phe1-Tyr3-octreotate. *Eur J Nucl Med Mol Imaging.* 2010;37:212-225.
26. Sgouros G, Squeri S, Ballangrud ÅM, et al. Patient-specific, 3-dimensional dosimetry in non-Hodgkin's lymphoma patients treated with 131I-anti-B1 antibody: assessment of tumor dose-response. *J Nucl Med.* 2003;44:260-268.

FIGURE LEGENDS

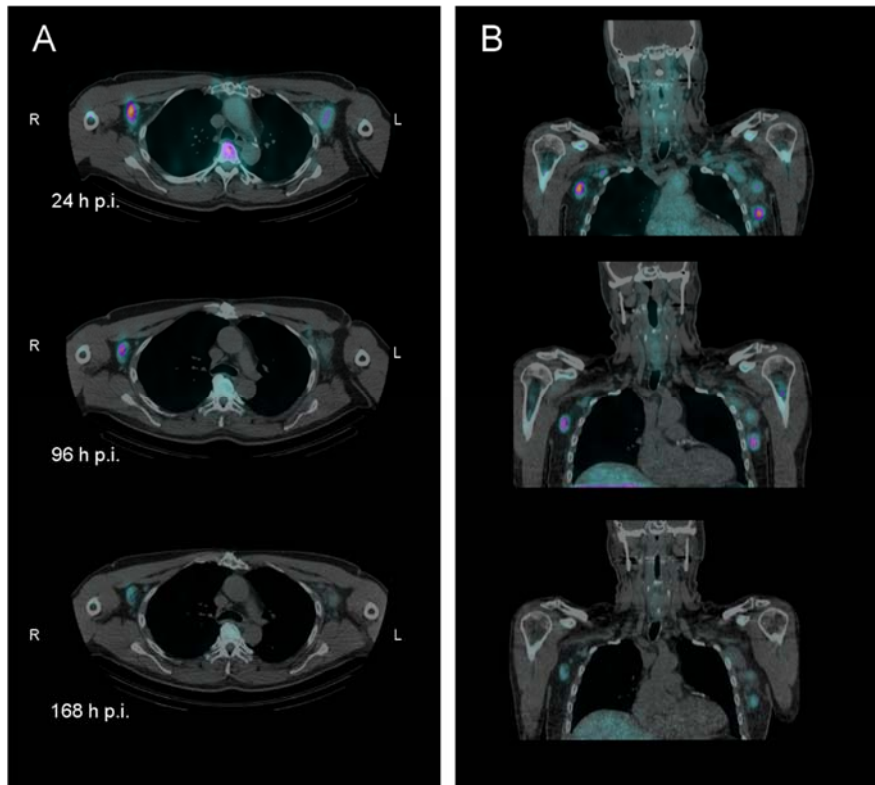


FIGURE 1. Axial (A) and coronal (B) SPECT/CT-fused images of patient 13 at three time points after administration of ^{177}Lu -lilotomab satetraxetan. Tumor 13b can be seen in the left axilla, and 13c in the right. The tumor dosimetry was based on multiple SPECT/CT-scans.

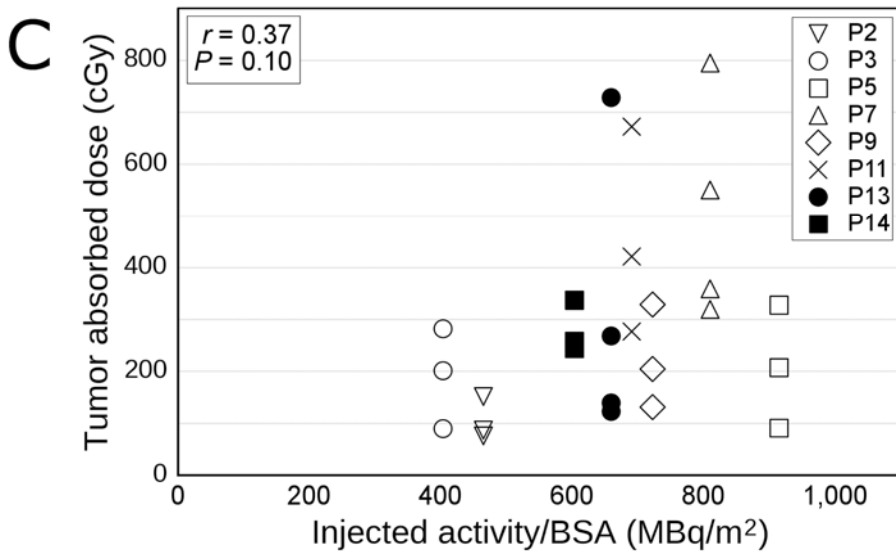
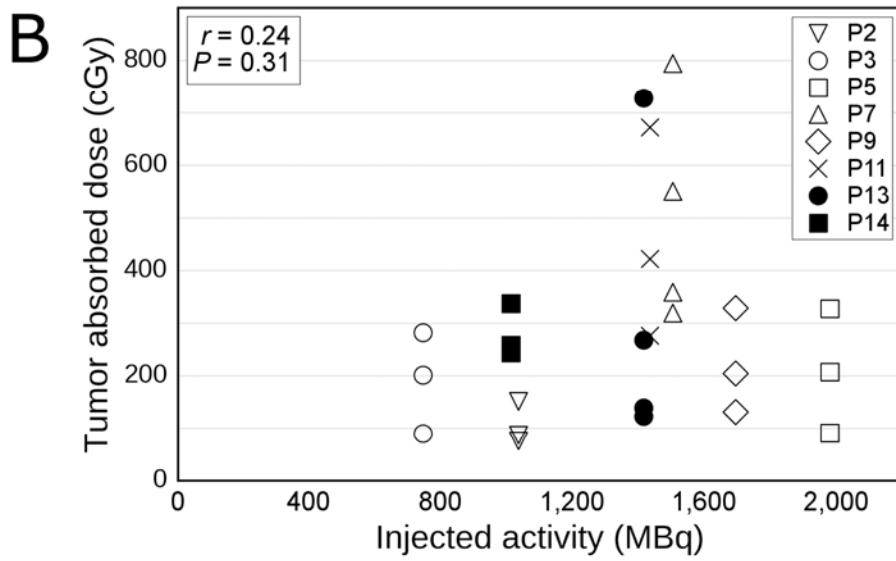
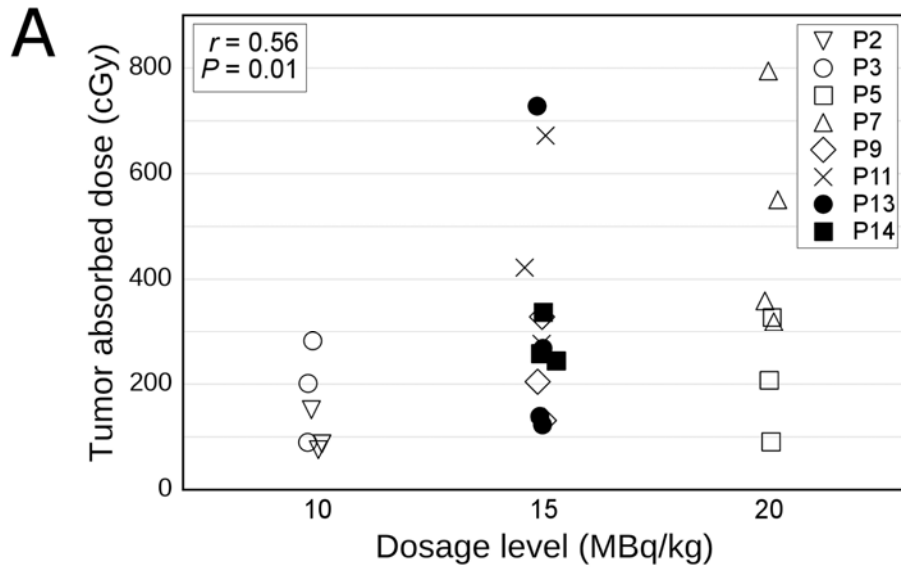


FIGURE 2. Tumor absorbed dose related to several parameters. Each symbol represents a tumor, and filled and open symbols represent arm 1 and 2, respectively. (A) Absorbed doses versus administered activity normalized by body weight (dosage level). The patients in this study were treated according to this dosage method. (B) Absorbed dose versus total administered activity. (C) Absorbed dose versus administered activity normalized by BSA. The latter two represent hypothetical dosage regimes.

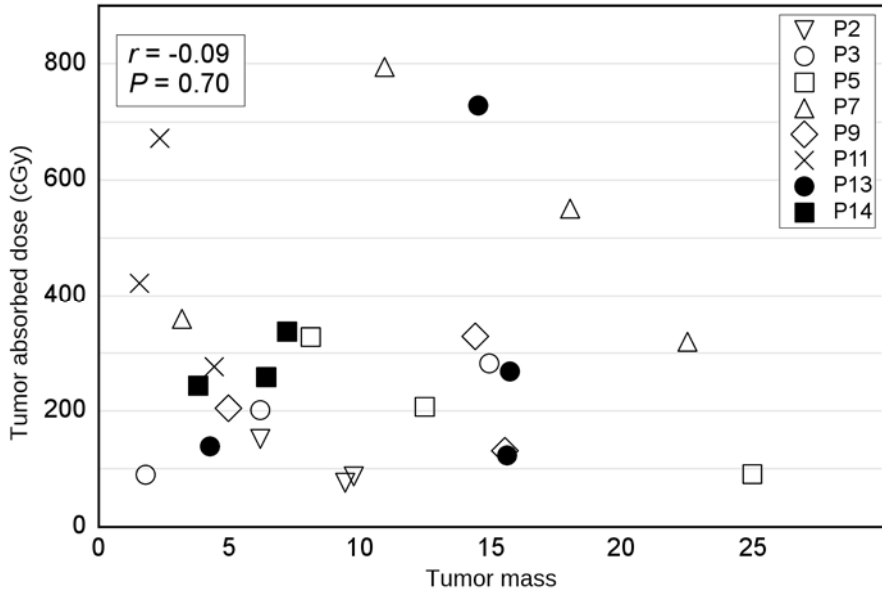


FIGURE 3. Tumor absorbed dose plotted against individual tumor mass. Filled and open symbols represent tumors belonging to patients in arm 1 and 2, respectively. Interestingly, no correlation was found between absorbed dose and tumor mass.

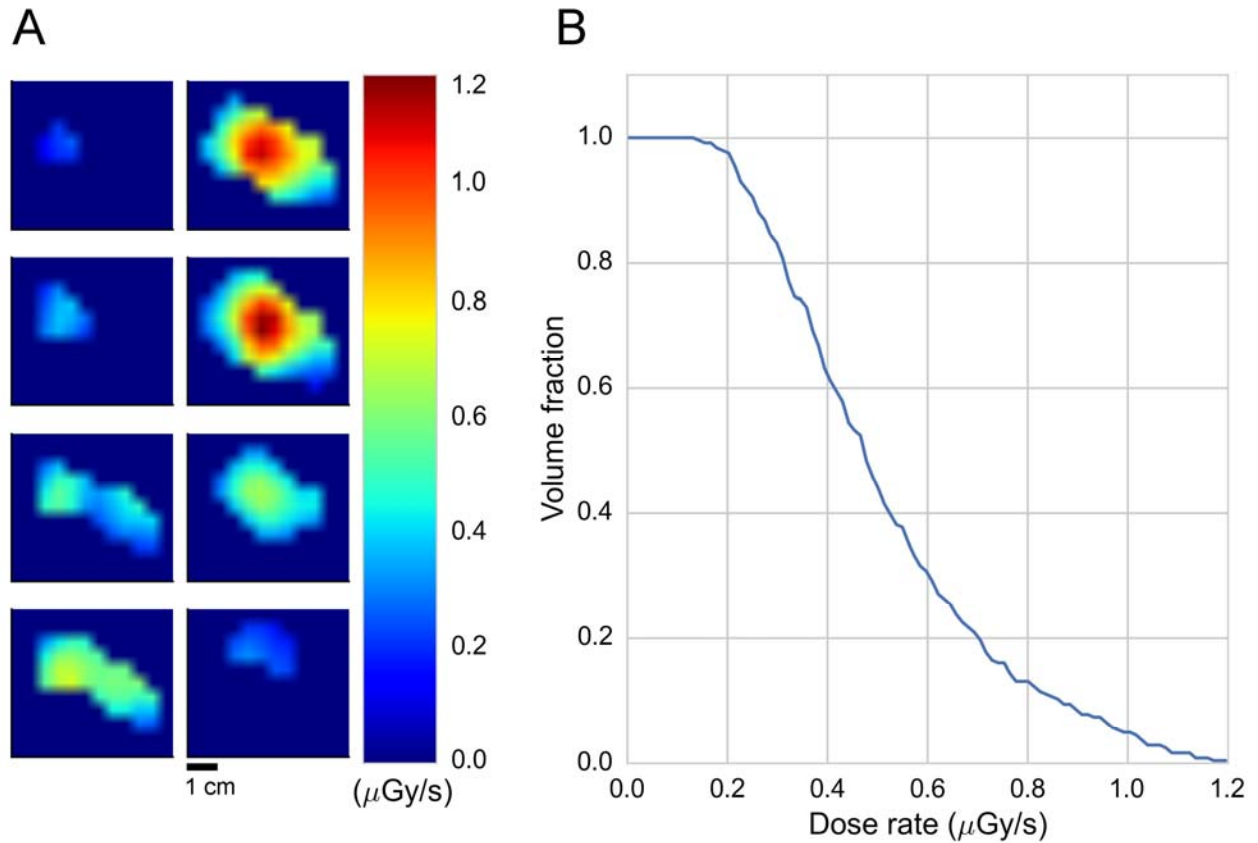


FIGURE 4. (A) Voxel dose rate map illustrated for tumor 5b; a subcutaneous tumor residing in the right nates area of patient 5. Eight axial slices show the tumor volume superior to inferior. The color bar indicates the dose rate of the different voxels. (B) The corresponding cDRVH shows the dose rate to different volume fractions of the tumor. E.g. a dose rate of about 0.5 $\mu\text{Gy/s}$ covers half of the tumor.

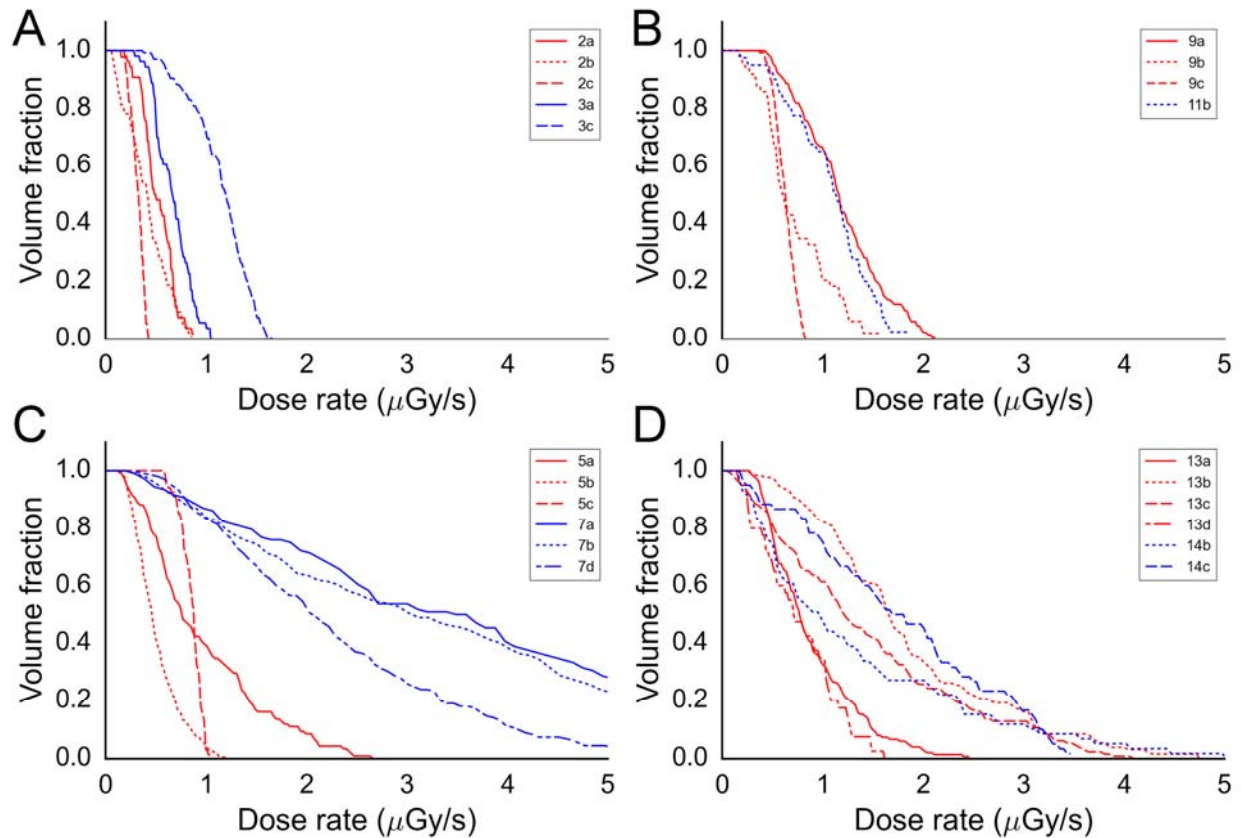


FIGURE 5. cDRVHs of the individual tumors included for voxel dosimetry. The histograms show the minimum dose rate to different fractions of the tumor volumes. Tumors are grouped by dosage level; 10, 15, 20 MBq/kg arm1 and 15 MBq/kg arm 2 in panel A, B, C and D respectively. The two colors in each panel represent the two patients included at each dosage level. Absolute size and position of each tumor can be found in Table 2 and dose rates in Table 3.

TABLES

TABLE 1. Patients included for the tumor dosimetry. Pre-treatment with rituximab (R) and pre-dosing (lilotomab) are indicated.

Patient	Sex	Dosage level (MBq/kg)	Inj activity MBq	Pre-treatment	BSA m ²
2	Male	10	1036	R + lilotomab	2.23
3	Male	10	746	R + lilotomab	1.85
5	Male	20	1982	R + lilotomab	2.17
7	Male	20	1505	R + lilotomab	1.86
9	Male	15	1696	R + lilotomab	2.35
11	Male	15	1435	R + lilotomab	2.08
13	Male	15	1416	R	2.15
14	Female	15	1013	R	1.68

TABLE 2. Tumor characteristics and mean tumor absorbed doses.

		Tumor Mass (g)	Effective half life (days)	Dose (cGy)	Dose/Injected activity (mGy/MBq)
2a	Neck R. Lower	6.2	2.9	151	1.5
2b	Neck R. Upper	9.8	3.0	87	0.8
2c	Para-esophageal	9.4	5.4	75	0.7
3a	Para-tracheal R.	6.2	4.7	201	2.7
3b	Neck L. Lower	1.8	8.1	90	1.2
3c	Para-vertebral R.	14.9	3.3	282	3.8
5a	Inguinal R.	12.5	3.4	207	1.0
5b	Subcut Nates R.	25.0	3.7	90	0.5
5c	Retroperitoneum	8.1	4.0	327	1.6
7a	Inguinal L. Middle	10.9	4.2	794	5.3
7b	Inguinal L. Upper	18.0	3.3	550	3.7
7c	Inguinal R.	3.2	3.8	359	2.4
7d	Inguinal L. Lower	22.5	3.3	320	2.1
9a	Mediastinum Anterior	14.4	4.2	328	1.9
9b	Inguinal R.	5.0	3.2	204	1.2
9c	Mediastinum R. Upper	15.5	2.0	130	0.8
11a	Axilla L.	2.3	4.2	672	4.7
11b	Neck R.	4.4	3.1	277	1.9
11c	Inguinal L.	1.5	3.9	422	2.9
	Mean values arm 1	10.1			2.2
13a	Axilla L. Lower	15.7	2.0	268	1.9
13b	Axilla L. Upper	15.6	2.5	123	0.9
13c	Axilla R. Lower	14.5	2.4	728	5.1
13d	Axilla R. Upper	4.3	2.9	139	1.0
14a	Inguinal R.	3.8	2.7	245	2.4
14b	Inguinal L. Lower	6.4	2.6	259	2.5
14c	Inguinal L. Upper	7.2	3.1	338	3.3
	Mean values arm 2	9.6			2.5

TABLE 3. Minimum dose rates covering 10, 50 and 90 % of the tumor volumes.

Tumor	\dot{D}_{10} ($\mu\text{Gy/s}$)	\dot{D}_{50} ($\mu\text{Gy/s}$)	\dot{D}_{90} ($\mu\text{Gy/s}$)
2a	0.7	0.5	0.3
2b	0.7	0.4	0.1
2c	0.4	0.3	0.2
3a	0.9	0.7	0.5
3c	1.5	1.2	0.7
5a	1.9	0.8	0.3
5b	0.9	0.5	0.3
5c	1.0	0.9	0.7
7a	7.1	3.7	0.9
7b	6.8	3.1	0.8
7d	4.1	2.1	0.9
9a	1.8	1.2	0.6
9b	1.3	0.6	0.3
9c	0.8	0.6	0.5
11b	1.6	1.2	0.6
13a	1.5	0.8	0.4
13b	3.1	1.7	0.8
13c	3.2	1.2	0.3
13d	1.3	0.7	0.3
14b	3.2	1.0	0.3
14c	3.2	1.8	0.4